Non-volatile Liquid Controlled Adiabatic Silicon Photonics Switch

Herbert D'heer, Cristina Lerma Arce, Stijn Vandewiele, Jan Watté, Koen Huybrechts, Roel Baets, and Dries Van Thourhout

Abstract—A broadband and non-volatile liquid controlled silicon photonics switch is designed and fabricated. The switch consists of an adiabatic coupler where the oxide above one of the waveguides is removed. Switching is realized by exposing this waveguide to liquids with different refractive indices. The switch design is based on self-consistent orthogonal coupled-mode theory. The measured crosstalk (XT) of a $1.4\,\text{mm}$ long switch is less than $-38\,\text{dB}$ and $-11\,\text{dB}$ over a $100\,\text{nm}$ wavelength range for bar and cross state, respectively. The insertion loss (IL) is less than $1\,\text{dB}$. Also the influence of the silicon waveguide thickness and the difference in liquid refractive indices on the switch performance is studied. Furthermore, an improved performance in cross state is demonstrated when a switch is actuated by a gas and a liquid. With a gas-liquid system a very large difference in cladding refractive index can be obtained.

Index Terms—Couplers, integrated optics, liquids, optical fiber communication, optical switches, silicon photonics.
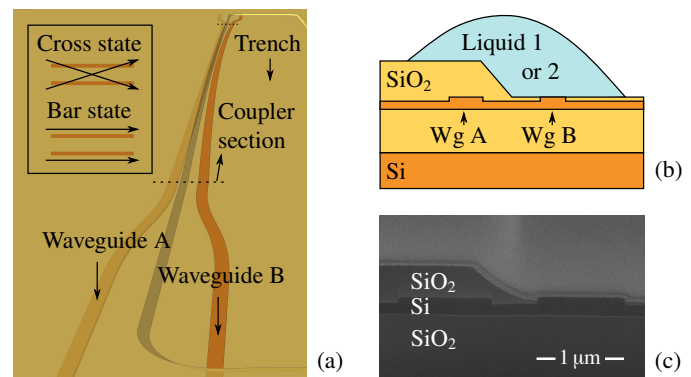

Figure 1: (a) Drawing of a liquid controlled adiabatic switch and (b) corresponding cross-section; (c) SEM image of cross-section at middle of coupler.

I. Introduction

DIFFERENT approaches exist to realize broadband integrated optical switches. One approach is using the electro-optic and thermo-optic effect to introduce a small change in refractive index [1], [2]. Another approach is to change the distance between waveguides such as in MEMS switches [3]. All previously designed switches are volatile, however.

The switching operation can also be realized by bringing liquids with a different refractive index near the switch structure. Liquids can be stored in a certain position without the need to add electrical energy. Therefore, they allow the realization of non-volatile switches [4]. Furthermore, liquids can have a large difference in refractive index which is advantageous in high index-contrast silicon photonic platforms. An even higher difference in refractive index, and better performance, can be obtained when a liquid and a gas are interchanged.

Non-volatile liquid controlled switches can be of particular interest in applications where the continuous operation of the switch is more important than the switching speed. One example of use could be in the management of the fiber network infrastructure in access networks. In these fiber networks

several wavelength bands need to be switched simultaneously which requires a broadband switch operation while allowing switching speeds on the order of milliseconds.

II. Concept and design

The switch we present consists of a 2×2 adiabatic coupler and is actuated by liquids. In an adiabatic coupler the light remains in one of the modes of the coupled system, but not necessarily in the same waveguide. Compared to interferometric structures it has a lower sensitivity to wavelength, temperature and fabrication tolerances. The disadvantage is a larger footprint, however.

A drawing of the switch and a cross-section are shown in Fig. 1(a) and (b), respectively. The switch is actuated by two liquids with a different refractive index. The two switch states (cross and bar state) and the direction of the guided light are schematically shown in the inset of Fig. 1(a). The oxide cladding on top of the coupler is locally removed by an etching process to expose one of the waveguides of the coupler to a changing medium. The oxide wall is slanted and the oxide is removed up to the same level as the top of the Si waveguides. By applying liquids with a different refractive index on top of the coupler, the effective index of the exposed waveguide changes. The liquids can be moved above the coupler by e.g. a liquid pump or electrowetting actuation. The advantage of these systems is that the liquid can remain on top of the coupler without consuming electrical power between two subsequent switching actions. An electrowetting-on-dielectric (EWOD) system suitable to actuate the switches is demonstrated in [5] and should allow switching times on the order of milliseconds. The additional footprint of these EWOD
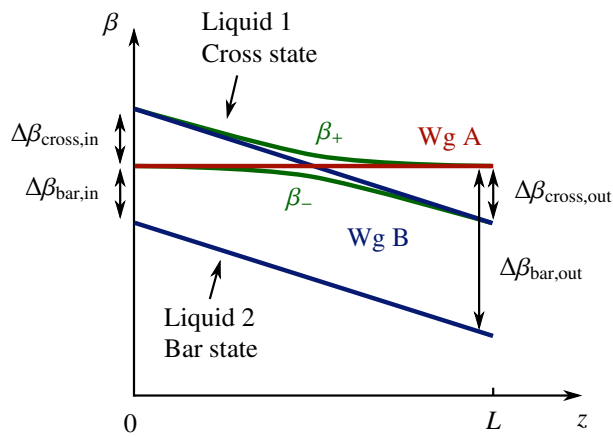
Figure 2: Diagram of propagation coefficients as a function of distance along the length of the coupler for cross and bar state.

Figure 3: Performance merit of liquid controlled couplers with a different waveguide geometry for a wavelength of 1550 nm.

structures can be small. For example, a 16×16 switch with 0.6 mm long couplers could have a footprint of about 13 mm $\times$ 13 mm. This includes the space required for electrodes, electrical traces, and barriers to separate the liquid droplets.

The propagation coefficients, β, of the individual waveguides are schematically shown in Fig. 2: in red for the waveguide covered by oxide, and in blue for the uncovered waveguide exposed to the liquids. The latter waveguide varies in width and hence its propagation coefficient varies along the length of the structure. In the example given here the cross state is realized by the high index liquid. $\Delta\beta$ indicates the difference in the propagation coefficients between the two waveguides at the ends of the coupler. In the cross state, the propagation coefficients of the two individual waveguides cross each other at the middle of the coupler. The propagation coefficients of the coupled system form an anti-crossing (shown in green in Fig. 2) and light is coupled to the neighboring waveguide. In the bar state, the propagation coefficients of the two individual waveguides do not cross. The propagation coefficients of the coupled system are approximately identical to those of the individual waveguides and light remains in the same waveguide. The oxide thickness above one of the waveguides needs to be large enough such that the propagation coefficient of this waveguide does not change when a liquid is on top.

When it is desired to integrate liquid couplers in dense switch networks it is advantageous to develop a design strategy which minimizes the insertion loss (IL) and crosstalk (XT) over a certain wavelength range while keeping the coupler length as small as possible. For this reason the couplers are designed following a self-consistent orthogonal coupled mode theory as described in [6]. This semi-analytical approach allows to design couplers in an efficient way.

We restrict ourselves to photonic integrated circuits in silicon-on-insulator (SOI). Obvious variables are the width, height and etch depth of the waveguides and the refractive indices of the liquids. We also restrict ourselves to couplers in which the two Si waveguides have an identical height and etch depth so as not to complicate the fabrication. Once a certain waveguide height 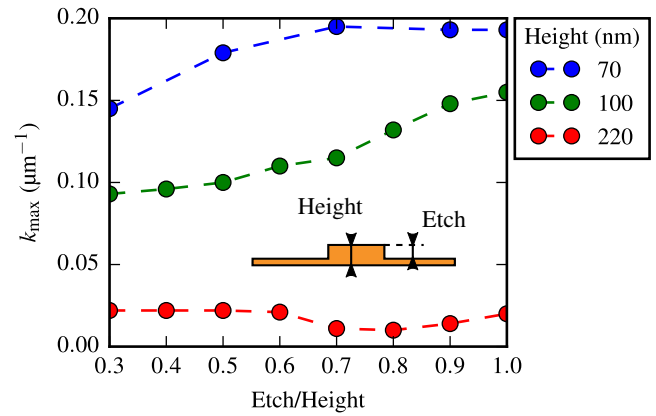and etch depth is chosen, the goal is then to control the waveguide widths and gap between the waveguides to achieve the lowest XT and IL for the same coupler length.

For a certain waveguide height and etch depth the waveguide widths at the coupler ends are obtained by maximizing

$$k = \min\{\Delta\beta_{\text{cross,in}}, \Delta\beta_{\text{bar,in}}, \Delta\beta_{\text{cross,out}}, \Delta\beta_{\text{bar,out}}\} \qquad (1)$$

over the widths of the two waveguides. This maximum is denoted by k_{max}. A large difference in propagation coefficients at both ends of the coupler and for the two switch states is beneficial as will be shown later. The minimum and maximum waveguide widths are restricted such that only one quasi TE mode is supported and such that the propagation loss is acceptable.

A large k_{max} can be realized by liquids with a large difference in refractive index and by optimizing the cross-section geometry of the waveguide. Therefore, it is instructive to evaluate k_{max} for different waveguide geometries. In Fig. 3 k_{max} is shown as a function of etch depth to waveguide height ratio for different waveguide heights and for a wavelength of 1550 nm. The minimum waveguide width is taken as 300 nm and the refractive indices of the liquids are chosen to be 1.42 and 1.63. Better performance is achieved for a larger difference in the liquid refractive indices. However, in practical realizations the liquids have preferably a high boiling point, low melting point, low vapor pressure and a high stability. Several liquids exist with these characteristics and with a refractive index around 1.42 and 1.63 [5]. Liquids with a larger difference in refractive index might not meet all requirements. From Fig. 3 it can be observed that a thinner waveguide gives a larger k_{max}. The performance of couplers with thick Si waveguides is limited by the difference of the effective refractive index of the waveguide exposed to the liquid in the two switch states. The overlap of the optical mode with a liquid is larger for a waveguide with reduced thickness which increases k_{max}.

For a coupler which should operate over a certain wavelength range $[\lambda_{\text{min}}, \lambda_{\text{max}}]$, we define $k_{\text{max},\Delta\lambda}$ as the maximum of

$$\min_{\lambda \in \Delta\lambda} k(\lambda), \quad \Delta\lambda = [\lambda_{\text{min}}, \lambda_{\text{max}}], \qquad (2)$$
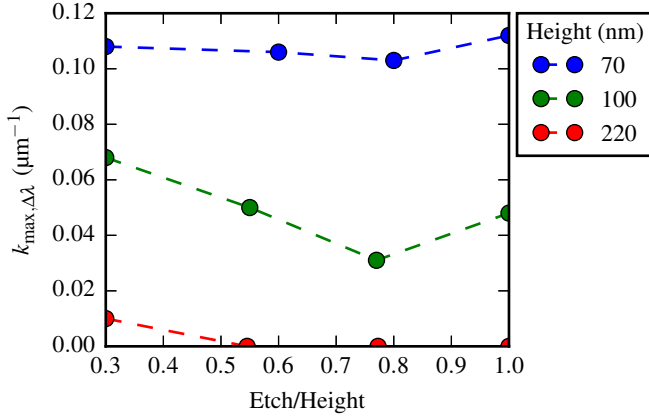
Figure 4: Performance merit of liquid controlled couplers with a different waveguide geometry over the wavelength range 1260 nm - 1650 nm.
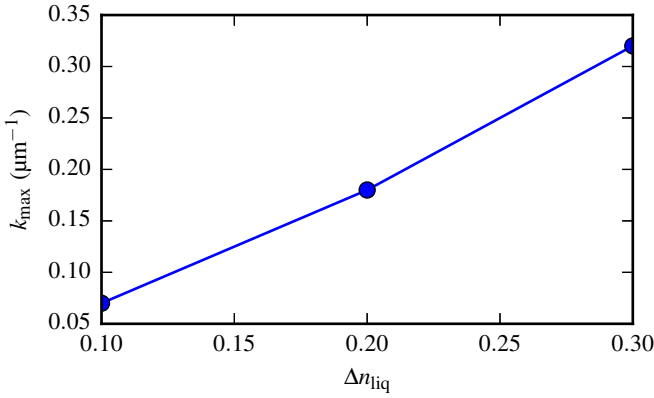

Figure 5: Relation between k_{max} and Δn_{liq} for a switch with 70 nm strip waveguides.

over all waveguide widths. It is often sufficient to calculate (2) only at λ_{min} and λ_{max}. In Fig. 4 $k_{max,\Delta\lambda}$ is shown for different waveguide geometries. The difference with Fig. 3 is that the wavelength range is from 1260 nm to 1650 nm. The liquids have again a refractive index of 1.42 and 1.63. For a waveguide height of 220 nm switching over the full wavelength range cannot be realized for all etch depths. To take into account fabrication tolerances the effect of width variations ($\pm\Delta w$) is also included in $k_{max,\Delta\lambda}$ by evaluating (2) over the widths $w \pm \Delta w$. Δw is taken as 10 nm in Fig. 4.

The value of k_{max} depends on the waveguide geometry, as shown earlier, but also on the refractive indices of the liquids. For Si couplers a larger difference in refractive index gives a better performance. The dependence of k_{max} on Δn_{liq} is shown in Fig. 5 for a waveguide with a thickness of 70 nm and for a wavelength of 1550 nm. A larger Δn_{liq} gives a substantially larger k_{max}.

Following the strategy of [7], the widths of the two waveguides along the length of the coupler are chosen such that in the cross state the difference between the propagation coefficients of the individual waveguides varies as

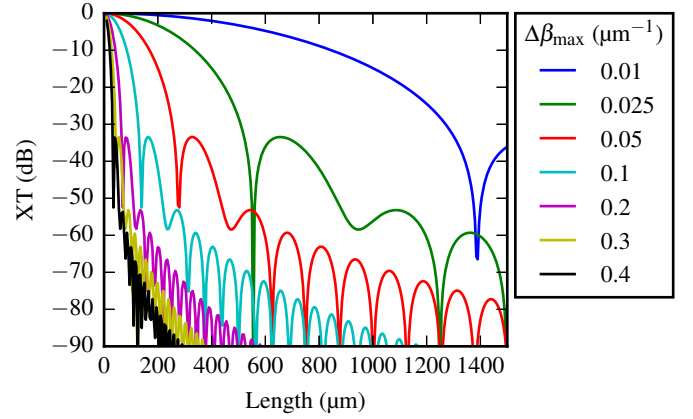$$\Delta\beta(z) = \Delta\beta_{max} \cos\theta(z), \tag{3}$$

Figure 6: XT for different values of $\Delta\beta_{max}$.

where $\theta(z)$ is chosen to be a Blackman function with $\theta(0) = 0$ and $\theta(L) = \pi$. $\Delta\beta_{max}$ is the maximum absolute difference between the propagation coefficients and consequently $\Delta\beta_{cross,in} = \Delta\beta_{cross,out} = \Delta\beta_{max}$. For a design at the wavelength 1550 nm this corresponds to k_{max} shown in Fig. 3. The gap between the two waveguides along the length of the coupler is obtained such that the coupling coefficient varies as

$$\kappa(z) = \kappa_{max} \sin\theta(z), \tag{4}$$

where κ_{max} is the maximum coupling coefficient. The ratio $\kappa_{max}/\Delta\beta_{max}$ is taken as 0.5. It is found that this gives the lowest XT. The coupling coefficient can be calculated as

$$\kappa^2 = \delta_\pm^2 - \delta_{12}^2, \tag{5}$$

$$\delta_\pm = \frac{\beta_+ - \beta_-}{2}, \tag{6}$$

$$\delta_{12} = \frac{\beta_1 - \beta_2}{2}, \tag{7}$$

where (β_+, β_-) and (β_1, β_2) are the propagation coefficients of the coupled system and individual waveguides, respectively. Alternatively, a more exact formula based on mode profiles can be used [6]. Once $\Delta\beta(z)$ and $\kappa(z)$ are determined, the XT and IL for a given coupler length can be calculated with the differential equation that describes the evolution of the modal amplitudes a_+ and a_-

$$-i\frac{\partial}{\partial z}\begin{pmatrix}a_+(z)\\a_-(z)\end{pmatrix} = \begin{pmatrix}\beta_+(z) & i\xi_\pm(z)\\-i\xi_\pm(z) & \beta_-(z)\end{pmatrix}\begin{pmatrix}a_+(z)\\a_-(z)\end{pmatrix}. \tag{8}$$

The parameter $\xi_\pm$ is the non-adiabatic term and depends on $\Delta\beta$ and κ [6].

In Fig. 6 the XT is shown as a function of coupler length for different values of $\Delta\beta_{max}$. This figure shows that a larger $\Delta\beta_{max}$ gives a lower XT. At the ends of the coupler the field profiles of the coupled system are identical to the field profiles of the individual waveguides for both cross and bar state and therefore the XT is well approximated by

$$20\log_{10}|a_+(L)|, \tag{9}$$

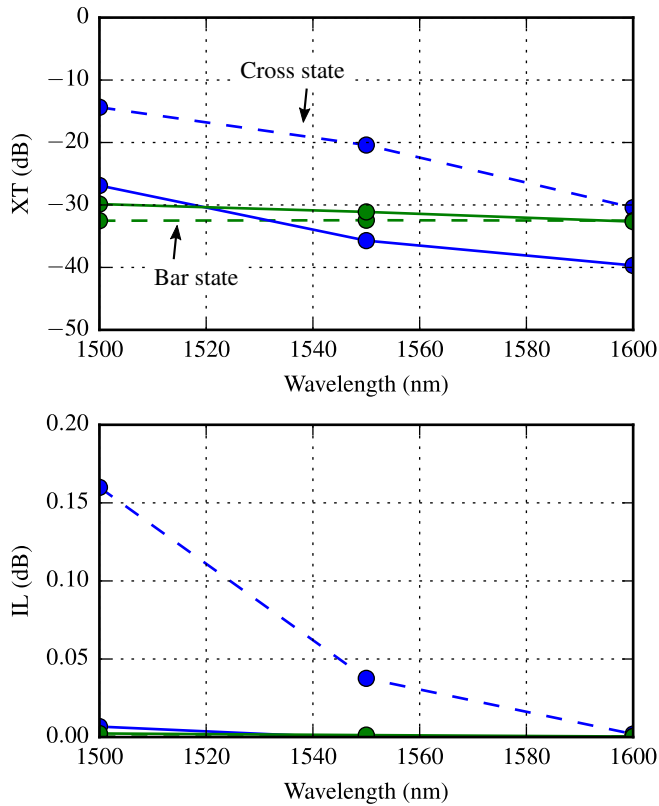with boundary conditions $(a_+(0), a_-(0)) = (0, 1)$.

Figure 7: Simulated transmission of the designed switch (solid lines) and the actually fabricated switch (dashed lines); blue: cross state, green: bar state. The switch has a length of 1410 μm and a waveguide height of 220 nm.

Figure 8: Simulated transmission of a switch with a length of 630 μm (solid lines) and 1410 μm (dashed lines); blue: corss state, green: bar state. The waveguide height is 70 nm.

III. DESIGN WITH 220 NM AND 70 NM THICK SILICON WAVEGUIDES

Switches with 220 nm and 70 nm thick waveguides are designed for liquids with refractive indices 1.42 and 1.63. These liquids define the bar state and cross state, respectively. Intrinsic waveguide losses are not included in the simulations. The performance of the generated switch geometries is verified by using the mode profiles ψ_+, ψ_- to calculate the non-adiabatic term. This gives a better approximation than when $\Delta\beta$ and κ are used. Propagation coefficients and mode profiles are simulated by a finite element mode solver [8].

The first switch design has 220 nm thick waveguides with a partial etch of 70 nm. This is in line with what is available from standard silicon photonics MPW platforms such as imec's platform [9]. The switch is designed at a wavelength of 1550 nm and has a length of 1410 μm. Fig. 7 shows the simulated XT and IL of the designed and fabricated switch. The thickness of the SiO$_2$ top-cladding above the covered waveguide is 450 nm and is large enough such that the effective index of this waveguide is not influenced by the liquids. These simulations show that for this switch it should be possible to have an IL below 0.02 dB and a XT better than −25 dB over a bandwidth of 100 nm for both cross and bar state. The layout of the coupler is shown in Fig. 1(a) and the minimum gap between the two waveguides is 525 nm. The separation of the waveguides at the end of the coupler is further increased to avoid that light couples between the waveguides which connect
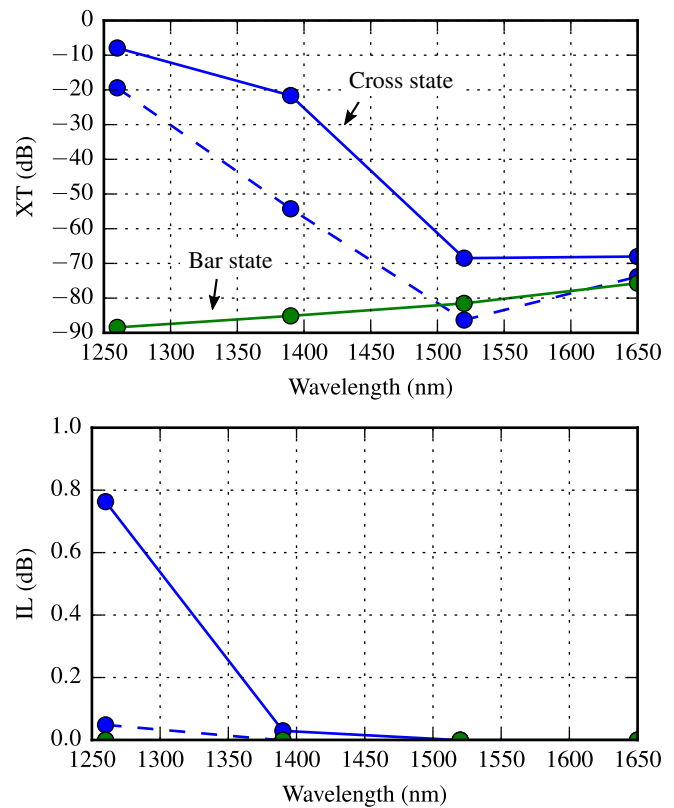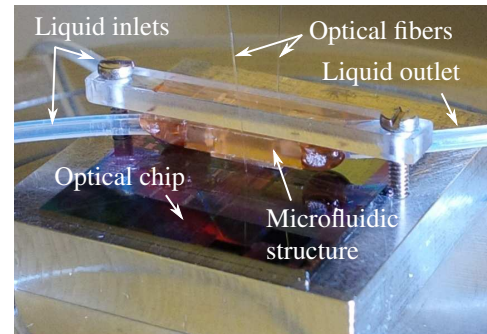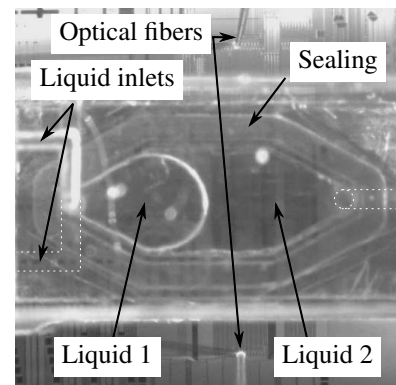

(a)

(b)

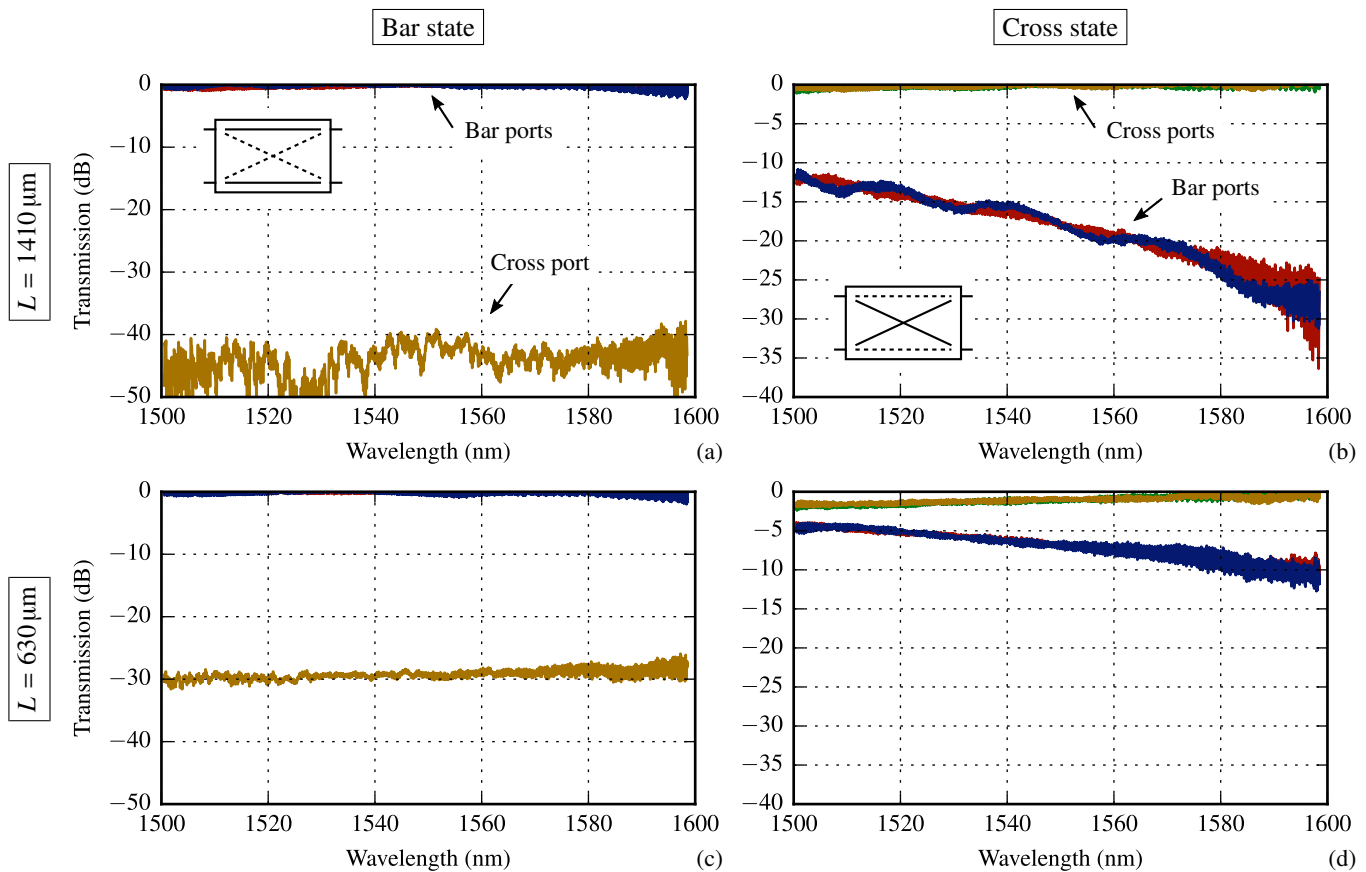Figure 9: Microfluidic structure mounted on an SOI chip: (a) side view and (b) top view.

Figure 10: Measured transmission of a fabricated switch in bar and cross state with a length of (a, b) 1410 μm and (c, d) 630 μm.

the coupler section to fiber grating couplers (FGCs).

The second switch has 70 nm thick strip waveguides and is designed to cover the wavelength range 1260 nm - 1650 nm. Simulation results are shown in Fig. 8 for two coupler lengths: 630 μm and 1410 μm. The lower range of the XT in the figure is limited to −90 dB because in practical situations the XT will likely be higher due to light scattering. As can be seen the performance is better for a reduced waveguide thickness, even for the shorter switch with a length of 630 μm. The geometry is generated at the wavelength 1610 nm with $\Delta\beta_{max} = 0.164\,\mu m^{-1}$. The design of the coupler could be improved such that the XT and IL are more symmetric over the wavelength range. This could be done by multiplying k in (2) by a wavelength dependent factor.

Both switch designs perform well in the bar state, with a low IL and XT over a large wavelength range. This is particularly interesting in switch networks where most couplers can be in bar state such as in a crossbar or a path-independent insertion-loss switch.

IV. Fabrication

SOI wafers with 70 nm thick Si and a sufficiently thick buried oxide are not readily available. Therefore only switches with 220 nm thick Si waveguides, as described in the previous section, are fabricated. The fabrication is done on SOI with 2 μm buried oxide and a 220 nm silicon top layer using 193 nm optical lithography [10]. The waveguides are defined by a 70 nm partial etch. The wafers are obtained through an imec-ePIXfab MPW run [9]. All waveguides are covered by a SiO_2 layer which is planarized and uniformly etched to a thickness of 450 nm. A trench is then created above one of the waveguides by optical lithography and buffered oxide etching (BOE). A scanning electron microscope (SEM) picture of a cross-section at the middle of the coupler is shown in Fig. 1(c).

The deposition of the oxide top-cladding is done by a high density plasma vapor deposition (HDPVD) process to obtain a good uniformity resulting in a uniform etch rate with BOE and a constant oxide slope geometry along the length of the coupler. BOE is preferred over dry etching due to its high selectivity between SiO_2 and Si. A second advantage is the obtained geometry of the oxide wall. A slope close to 90° and sharp edges are not preferred to reduce the risk that the liquids are not fully substituted. An oxide wall with a small slope is also not preferred. This makes the propagation coefficient of the shielded waveguide more dependent to the refractive index of the liquids which reduces the performance.

The etch stop-level is controlled by repeatedly measuring the surface topology while the SiO_2 above the Si waveguide is being removed. When a height difference of about 35 nm is obtained between the top of the Si waveguide and the etched SiO_2 next to it, the etching is stopped.

V. Characterization

The transmission spectra of the switches are obtained by applying a liquid drop on top of the chip or by alternating two liquids in a polyphenylsulfone microfluidic structure mounted on top of the chip (see Fig. 9). The microfluidic structure is provided by Bartels Mikrotechnik GmbH. In this structure two liquids are alternately injected by two separate inlet channels and fill a chamber located above the switch. FGCs are not covered by liquids or the microfluidics structure such that the switch can be easily characterized with optical fibers. Liquids with a refractive index of 1.42 and 1.63 are provided by Cargille Laboratories (Series AA, n_D: 1.430 and Series B, n_D: 1.666) [11]. Other liquid properties, different than the refractive index, are less relevant for this work. The transmission measurements are normalized with respect to a reference waveguide to exclude the response of the FGCs. The input laser light is TE polarized.

Measurement results of switches with a different length are shown in Fig. 10. In Fig. 10(a) a $1410\,\mu m$ long switch is in bar state with a low index liquid (n_{liq} = 1.42) on top. The XT is lower than $-38\,dB$ from $1500\,nm$ to $1600\,nm$. In Fig. 10(b) the same switch is in cross state with a high index liquid (n_{liq} = 1.63) on top. The XT is lower than $-11\,dB$. The IL for cross and bar state over the measured wavelength range is lower than $1\,dB$ after normalization. The wavelength range is restricted by the wavelength range of the tunable laser and the bandwidth of the FGCs. The XT in bar state, shown in Fig. 10(a), could be restricted by the XT introduced by the FGCs which is around $-40\,dB$ for two isolated waveguides with the same position of the FGCs. In Fig. 10(c) and (d) the transmission of a $630\,\mu m$ long switch is shown. It can be seen that the performance is better for longer switches.

The average IL and standard deviation of a nominal identical switch on 3 different dies is shown in Fig. 11 for the two switch lengths. The 2 cross-port or bar-port spectra for each switch state are averaged to obtain the IL of one switch. The larger uncertainty starting from a wavelength of $1580\,nm$ is due to the limited bandwidth of the FGCs. The spectra are first filtered with a low-pass filter to remove parasitic effects such as reflections at the FGCs.

The simulated transmission spectra of the actually fabricated switch are shown in Fig. 7 in dashed lines. The difference with the designed switch is the geometry of the oxide slope and the oxide over-etch. The measured and simulated spectra correspond well. In bar state the measured XT is roughly $8\,dB$ lower than the simulated.

In Fig. 12 measurements are shown for 3 different nominal oxide-trench offsets $(-250, 0, 250)\,nm$ for a $1410\,\mu m$ long coupler in cross state. The definition of the oxide offset is shown in the inset of the figure. The influence of such an offset is limited to a few dB variation in XT. It is expected that for an advanced lithography system the position of this slope can be well controlled within this range. Therefore the proposed switch is sufficiently tolerant to such variations.

A system with two different liquids is useful when the liquids are moved by electrowetting, both in terms of reducing the drive voltage and the stability against mechanical shock.
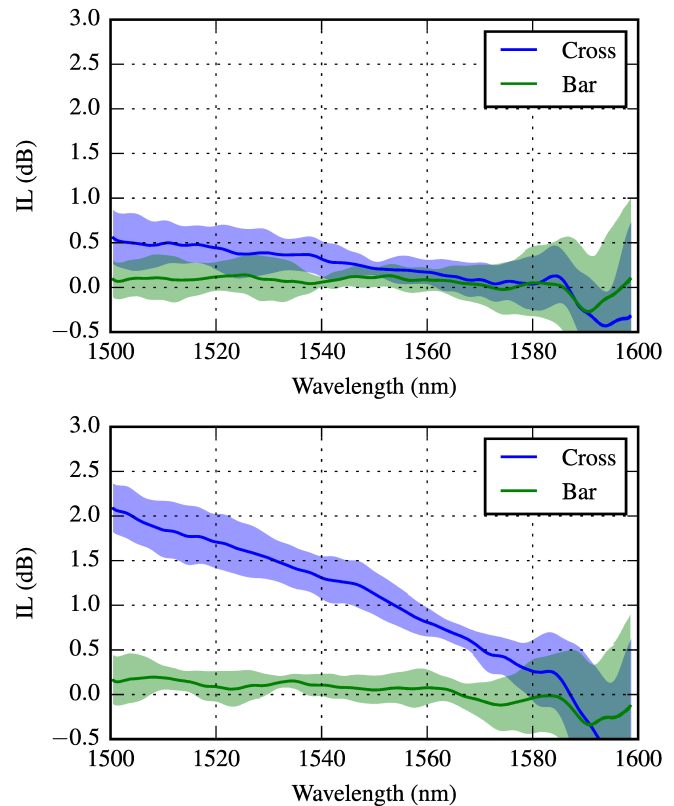

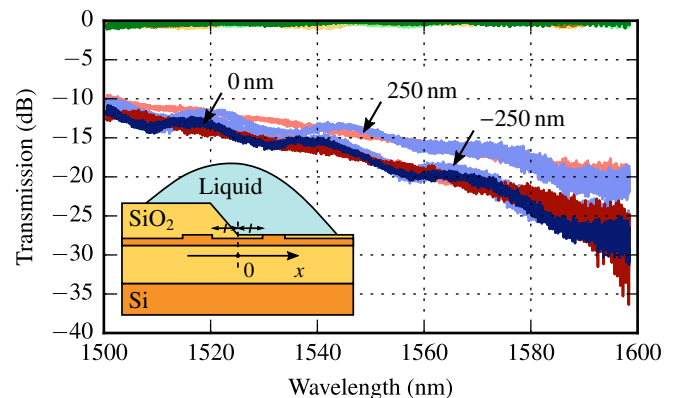Figure 11: Cross- and bar-state IL of a switch with a length of (a) $1410\,\mu m$ and (b) $630\,\mu m$.

Figure 12: Measured transmission of a $1410\,\mu m$ long coupler in cross sate for different oxide trench offsets. The two cross-port and bar-port spectra are shown per trench offset.

A system whereby the liquid drop is surrounded by a gas will typically increase the required actuation voltage, but allows for a higher index contrast and hence improved performance. In such a system the liquid and gas are the high and low index medium, respectively. Using the same method as described above, a coupler is designed for a liquid with a refractive index of 1.42 as the first cladding medium, and air as the second cladding medium. The measurements of the two states are shown in Fig. 13. The difference in refractive index between the two changeable media is increased from 0.21 for the liquid-liquid switch to 0.42 for the liquid-air switch. The performance
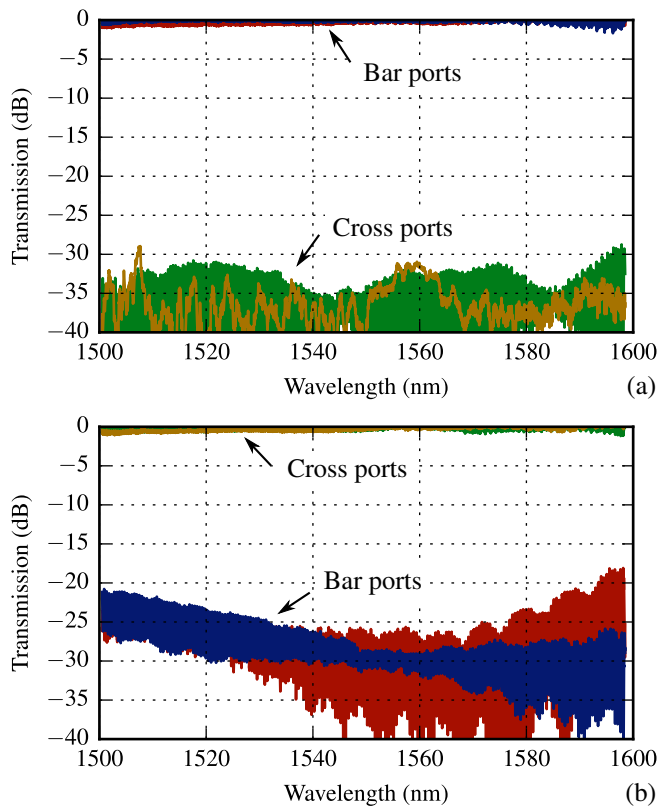
Figure 13: Measured transmission of a liquid-air switch with a length of 1410 μm; (a) bar state with air cladding and (b) cross sate with liquid cladding.

is considerably improved: the measured XT in cross state now is better than 20 dB over the 100 nm wavelength range. A liquid with a higher refractive index could further increase the performance.

VI. Conclusion

A new concept of a liquid controlled, non-volatile bistable adiabatic 2×2 switch has been proposed and demonstrated. The switch actuation is performed by two liquids with a different refractive index applied sequentially on top of the coupler. By exposing one waveguide of an adiabatic coupler structure to the liquids, a switch element was realized with good performance over a wide bandwidth. An extensive design optimization has been done. Simulations show that for a standard 220 nm heigh waveguide an IL and XT less than 0.02 dB and −25 dB can be obtained, respectively, for both cross and bar state over a wavelength range of 100 nm and for a coupler length of 1.4 mm. The switches were fabricated with 220 nm SOI. We measured a XT lower than −38 dB in bar state and −11 dB in cross state and an IL lower than 1 dB over the wavelength range 1500 nm to 1600 nm.

Further optimisation of the cross-section and reducing the waveguide height to for example 70 nm should allow the switch to operate with good performance over the full telecommunication wavelength range, which is about 400 nm. Improved performance can also be achieved by using fluids with a larger refractive index difference. With a liquid and

gas, a large difference in refractive index can be obtained and an improved performance is observed in cross state. The corresponding measured XT of a fabricated coupler is less than −20 dB.

With these optimized designs, shorter coupler lengths of about 0.6 mm should be possible while still allowing good performance. In combination with an EWOD actuation system this could yield large-scale switch matrices, including at least 16×16 switches on a standard silicon photonics die. Therefore, adiabatic couplers actuated by liquids, with zero static power consumption, could be a promising alternative to previous optical switch approaches.

References

[1] Y. Silberberg, P. Perlmutter, and J. E. Baran, "Digital optical switch", *Applied Physics Letters*, vol. 51, no. 16, pp. 1230–1232, 1987.

[2] M. Hoffmann, P. Kopka, and E. Voges, "Thermooptical digital switch arrays in silica-on-silicon with defined zero-voltage state", *Journal of Lightwave Technology*, vol. 16, no. 3, pp. 395–400, 1998.

[3] T. J. Seok, N. Quack, S. Han, R. S. Muller, and M. C. Wu, "Large-scale broadband digital silicon photonic switches with vertical adiabatic couplers", *Optica*, vol. 3, no. 1, pp. 64–70, 2016.

[4] H. D'heer, C. Lerma Arce, J. Watté, K. Huybrechts, R. Baets, and D. Van Thourhout, "Broadband and non-volatile liquid controlled silicon photonics switch", in *CLEO*, San Jose, CA, USA, 2016, SM3G.6.

[5] S. Günther, C. Endrödy, S. Si, S. Weinberger, R. Claes, Y. Justo, H. D'heer, A. Neft, and M. Hoffmann, "EWOD system designed for optical switching", in *MEMS*, Las Vegas, NV, USA, 2017, pp. 1329–1332.

[6] H. Ishikawa, "Fully adiabatic design of waveguide branches", *Journal of Lightwave Technology*, vol. 25, no. 7, pp. 1832–1840, 2007.

[7] H. kai Hsiao, K. A. Winick, and J. D. Monnier, "Midinfrared broadband achromatic astronomical beam combiner for nulling interferometry", *Appl. Opt.*, vol. 49, no. 35, pp. 6675–6688, 2010.

[8] COMSOL, Inc. (2017), [Online]. Available: www.comsol.com.

[9] Europractice silicon photonics MPW. (2017), [Online]. Available: www.europractice-ic.com.

[10] S. K. Selvaraja, P. Jaenen, W. Bogaerts, D. Van Thourhout, P. Dumon, and R. Baets, "Fabrication of photonic wire and crystal circuits in silicon-on-insulator using 193-nm optical lithography", *Journal of Lightwave Technology*, vol. 27, no. 18, pp. 4076–4083, 2009.

[11] Cargille Laboratories, Inc. (2017), [Online]. Available: www.cargille.com.